Kinematic models of plate boundary deformation in southwest Iceland derived from GPS observations

Thóra Árnadóttir,[1] Weiping Jiang,[1,2] Kurt L. Feigl,[3] Halldór Geirsson,[4] and Erik Sturkell[1,4]

Received 27 June 2005; revised 29 March 2006; accepted 5 April 2006; published 8 July 2006.

[1] We use data from GPS campaign and continuous measurements from 1992 to 2004 in SW Iceland to map the surface velocity field from the Reykjanes Peninsula to the Eastern Volcanic Zone. We divide the time series into preseismic (July 1992 to June 2000) and postseismic (June 2000 to May 2004) time intervals, and we estimate GPS station velocities for each interval as well as coseismic offsets due to the June 2000 earthquake sequence in the south Iceland seismic zone (SISZ). In addition to the plate spreading, the preseismic velocity field shows the effects of inflation at Hengill and Hekla volcanoes, whereas the postseismic velocities show deformation following the June 2000 earthquakes. We consider several kinematic models to explain the preseismic velocities. Our preferred model includes several dislocations and point sources in an elastic half-space, with left-lateral slip along the plate boundary on the Reykjanes Peninsula and below the SISZ, opening across the Reykjanes Peninsula, and the Western and Eastern rift zones. The optimal model has a locking depth of about 8 km in the central and eastern part of the Reykjanes Peninsula with a deep slip rate of about 17 mm/yr and an opening of about 9 mm/yr. This locking depth is in agreement with the thickness of the seismogenic crust on the Reykjanes Peninsula, which appears to vary between 7 and 9 km. For the SISZ, we obtain a deep slip rate of about 19 mm/yr below 16 km depth, which is considerably deeper than the earthquake hypocenter depths in the area.

Citation: Árnadóttir, T., W. Jiang, K. L. Feigl, H. Geirsson, and E. Sturkell (2006), Kinematic models of plate boundary deformation in southwest Iceland derived from GPS observations, *J. Geophys. Res.*, *111*, B07402, doi:10.1029/2005JB003907.

1. Introduction

[2] Iceland is located on the Mid-Atlantic Ridge, between the Reykjanes Ridge in the south and the Kolbeinsey Ridge to the north. The island straddles the boundary of the North American and Eurasian plates. The motion across the plate boundary in the southwestern part of Iceland is accommodated by several volcanic rift zones and a transcurrent slip zone. The Reykjanes segment of the Mid-Atlantic Ridge comes onshore at the Reykjanes Peninsula oblique rift zone. At the Hengill triple junction, the rift branches into the Western Volcanic Zone (WVZ) and the south Iceland seismic zone (SISZ) (Figure 1). The SISZ is an E-W transform zone that accommodates sinistral shear as slip on many short vertical dextral N-S faults, spaced 1–5 km apart [*Einarsson et al.*, 1981; *Einarsson and Eiríksson*, 1982]. At the eastern edge of the SISZ, the plate motion is accommodated by rifting across the Eastern Volcanic Zone (EVZ). The EVZ extends northeastward, turning northward where the plate boundary continues as the Northern Volcanic Zone (NVZ). Farther north, the plate boundary extends offshore along the Tjörnes Fracture Zone (TFZ), a right-lateral transform zone that connects the NVZ and Kolbeinsey Ridge. One of Iceland's most active volcanoes, Hekla, is located near the intersection of the SISZ and the EVZ. From this intersection, an area of alkaline volcanism, the Eastern Volcanic Flank Zone extends toward the southwest, with geochemical and structural characteristics of a propagating rift [*Jóhannesson et al.*, 1990]. Several active volcanoes are in this area, including Katla volcano, that last erupted in 1918 and is currently showing signs of unrest [*Sturkell et al.*, 2003].

[3] GPS measurements have been used to observe crustal deformation Iceland since 1986. The complex region of southwest Iceland, including the Reykjanes Peninsula, the Hengill triple junction and the SISZ have been the focus of many surveys, and a fairly dense network of GPS stations now exists in the area (Figure 2). Two International GPS Service (IGS) stations are located in Iceland. The first station, REYK was installed in 1995 and a second station, HOFN, in 1997. A network of continuous GPS stations (ISGPS) began operating in early 1999 under the aegis of the Icelandic Meteorological Office (IMO) [*Árnadóttir et al.*, 2000; H. Geirsson et al., Current plate movements across the Mid-Atlantic ridge determined from 5 years of continuous GPS measurements in Iceland, submitted to *Journal of Geophysical Research*, 2005, hereinafter referred to as Geirsson et al., submitted manuscript, 2005]. The first four stations were installed in the Hengill area, due to

[1] Nordic Volcanological Center, Reykjavík, Iceland.
[2] Now at GPS Research Center, Wuhan University, Wuhan, China.
[3] Centre National de la Recherche Scientifique, Toulouse, France.
[4] Icelandic Meteorological Office, Reykjavík, Iceland.

0148-0227/06/2005JB003907$09.00

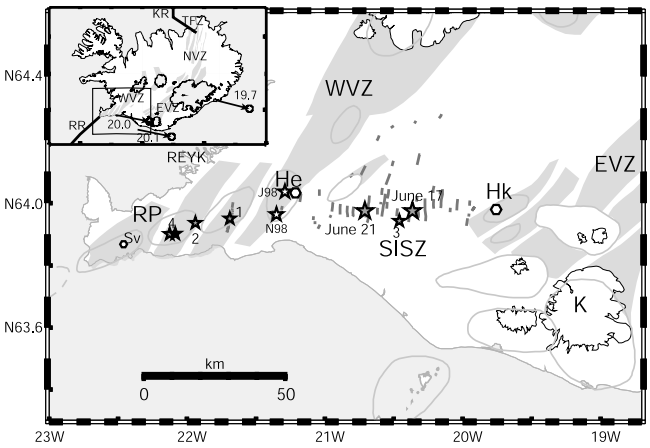

Figure 1. Map showing the main tectonic features of the study area: the Reykjanes Peninsula (RP), the Hengill triple junction (He), the Western Volcanic Zone (WVZ), the south Iceland seismic zone (SISZ), Hekla volcano (Hk), Katla volcano (K), and the Eastern Volcanic Zone (EVZ). The shaded areas show individual fissure swarms with associated central volcanoes. Mapped surface faults of Holocene earthquakes in the SISZ are shown with thick gray lines [*Einarsson and Smundsson*, 1987]. The epicenter locations of $M_w \geq 5$ earthquakes in 1998 (white stars), the June 2000 sequence (gray stars) and August 2003 (black star) are shown. The June 2000 main shocks and the largest triggered earthquakes are labeled (see also Table 1). Centers of deflation at Svartsengi (Sv) and inflation at Hengill (He) and Hekla (Hk) are shown with hexagons. The location of Reykjavík, the capital of Iceland, is labeled by REYK. The inset shows a simplified map of the plate boundary across Iceland, with the location of the study area indicated with a black rectangle. The Reykjanes Ridge (RR), Northern Volcanic Zone (NVZ), Tjörnes fracture zone (TFZ), and Kolbeinsey Ridge (KR) are labeled. The black arrows show the spreading directions and magnitudes (full rate in mm/yr) of the Eurasian plate relative to stable North America predicted by the REVEL plate motion model [*Sella et al.*, 2002].

increased seismic activity and inflation starting in 1993 [*Sigmundsson et al.*, 1997; *Feigl et al.*, 2000], culminating with two $M_w \sim 5$ earthquakes in 1998 [*Rögnvaldsson et al.*, 1998; *Árnadóttir et al.*, 1999; *Vogfjörd et al.*, 2005]. The activity in Hengill decreased in early 1999. As of June 2004, there were 17 continuous GPS stations operating in Iceland (Geirsson et al., submitted manuscript, 2005).

[4] GPS measurements from 1986 to 1992 confirm left-lateral shear strain accumulation of 0.2 μstrain/yr across the Reykjanes Peninsula [*Sturkell et al.*, 1994]. The horizontal deformation measured with GPS surveys in 1993 and 1998 along the Reykjanes Peninsula, has been modeled as a shear zone slipping at a rate of ~16.5 mm/yr below a locking depth of ~6.5 km, assuming a simple screw dislocation model [*Hreinsdóttir et al.*, 2001]. *Sigmundsson et al.* [1995] analyzed GPS measurements in the SISZ from 1989 to 1992 and estimated the current rate of extension across central south Iceland as 21 ± 4 mm/yr at N117° ± 11°E, assuming a steady velocity for the four year interval. From the analysis, they concluded that most (85% ± 15%) of the relative NUVEL-1 plate motion [*DeMets et al.*, 1990] across central Iceland is accommodated by the EVZ, with less than 15% of the motion taken up by the WVZ. This unequal distribution of motion led *Sigmundsson et al.* [1995] to postulate a Hreppar microplate on the north side of the SISZ transform zone between the EVZ and the WVZ, and that the SISZ transform zone accommodates the shear and counterclockwise rotation by "bookshelf faulting". According to this model, short faults striking essentially N-S delimit blocks that are approximately 5 km wide (E-W dimension) and 10–15 long (N-S). Boundary element modeling confirms that the array of mapped faults can accommodate the majority of the expected east-west transform motion across the SISZ if the N-S faults are at least 10 km long [*Hackman et al.*, 1990].

[5] GPS campaign measurements between 1994 and 2003 suggest a significant variation of spreading rates across the WVZ and the EVZ [*LaFemina et al.*, 2005]. The spreading rates across the EVZ decrease from 19.0 ± 2.0 mm/yr in the northeast to 11.0 ± 0.8 mm/yr in the southwest, whereas the rates increase in the WVZ from 2.6 ± 0.9 mm/yr in the northeast to 7.0 ± 0.4 mm/yr in the southwest. The sum of the extension rates in the direction of plate motion (N102°E) across the two rift zones is approximately 18–20 mm/yr, in agreement with models of plate motion [*DeMets et al.*, 1994; *Sella et al.*, 2002]. This result is consistent with the suggestion that the WVZ is less active and most of the spreading is presently occurring across the EVZ [*Einarsson*, 1991; *Sigmundsson et al.*, 1995].

[6] Numerous large ($M_S \geq 6$) earthquakes have occurred in the SISZ in historical time [*Einarsson et al.*, 1981]. The largest earthquake (M_w = 6.5) in the SISZ since 1912

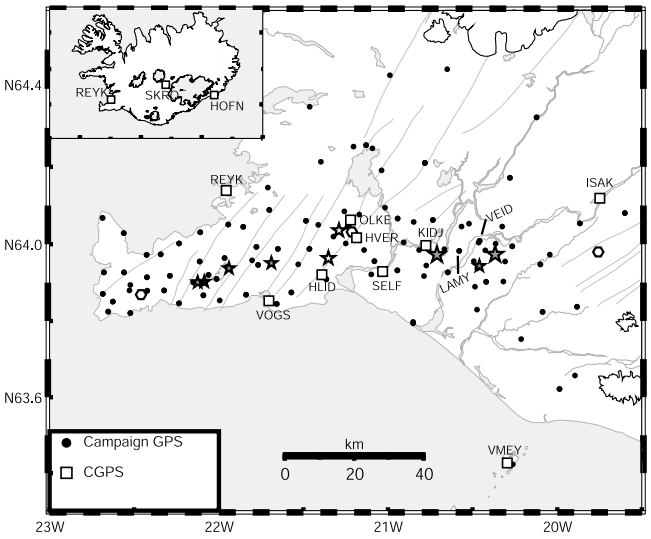

Figure 2. Locations of campaign GPS stations on the Reykjanes Peninsula and SISZ (black circles) and continuous GPS stations (open squares) used in this study. The thin gray lines show individual fissure swarms. The epicenters of $M_w \geq 5$ earthquakes are shown with stars, and white hexagons denote centers of inflation or deflation (see text for details). The inset shows the locations of the CGPS stations HOFN and SKRO.

Table 1. Deformation Events[a]

Event	Date	Time, UTC	Location	Radius, km
J98	4 Jun 1998	213653.811	21.290°W, 64.036°N	10
N98	13 Nov 1998	103834.415	21.352°W, 63.963°N	10
Hekla eruption	26 Feb 2000	180700	19.69°W, 63.995°N	10
J17	17 Jun 2000	154040.998	20.367°W, 63.973°N	120[b]
1	17 Jun 2000	154106.900	21.689°W, 63.951°N	120[b]
2	17 Jun 2000	154111.254	21.940°W, 63.937°N	120[b]
3	17 Jun 2000	154250.587	20.460°W, 63.943°N	120[b]
4	17 Jun 2000	154527.142	22.125°W, 63.901°N	120[b]
J21	21 Jun 2000	005146.985	20.711°W, 63.972°N	120[b]
Earthquake	23 Aug 2003	020012.764	22.086°W, 63.902°N	10

[a]Earthquake dates, times, and locations are from the SIL catalogue (B. Thorbjarnardóttir, personal communication, 2004). The radius is the radius of influence we assume for the events. We use a radius of 120 km and an average location (20.473°W, 63.999°N) for the June 2000 earthquake sequence. This allows us to use one radius for all six earthquakes considered.

[b]Distance from (20.473°W, 63.999°N). The earthquake labels in parenthesis refer to labeling in Figure 1.

occurred on 17 June 2000 (Figure 1) [*Stefánsson et al.*, 2003]. Seismicity increased over a large area in SW Iceland following the 17 June main shock, with at least four moderate size ($M_w \geq 5$) earthquakes occurring within 5 min of the main shock [*Vogfjörd*, 2003; *Antonioli et al.*, 2006]. One of the triggered events was located in the SISZ and three on the Reykjanes Peninsula (labeled 1, 2, 3, and 4 in Figure 1 and Table 1). A second large event ($M_w = 6.5$) occurred on 21 June 2000, about 17 km west of the 17 June main shock [*Stefánsson et al.*, 2003]. Crustal deformation signals from the June 2000 earthquake sequence were recorded by the continuous GPS network in Iceland [*Árnadóttir et al.*, 2000; Geirsson et al., submitted manuscript, 2005], campaign GPS measurements [*Árnadóttir et al.*, 2001, 2004], and interferometric analysis of synthetic aperture radar images (InSAR) [*Pedersen et al.*, 2001, 2003; *Pagli et al.*, 2003]. The geodetic data have been used to estimate the fault geometry and slip for the 17 and 21 June main shocks, both assuming uniform slip [*Árnadóttir et al.*, 2001; *Pedersen et al.*, 2001] and distributed slip [*Pedersen et al.*, 2003]. Interpretation of geodetic and seismic observations, as well as surface ruptures observed for the June 2000 earthquake sequence, confirm rupture on several near vertical, N-S structures with predominantly right-lateral strike-slip motion [*Pedersen et al.*, 2003, *Clifton et al.*, 2003; *Árnadóttir et al.*, 2004; *Hjaltadóttir et al.*, 2005; *Clifton and Einarsson*, 2005].

[7] In this paper we use campaign and continuous GPS data to estimate a surface velocity field in SW Iceland in the time interval 1992–2004. Several $M_w \geq 5$ earthquakes occurred during this time period in the study area (Figure 1 and Table 1). These are a $M_w = 5.4$ (International Seismological Centre (ISC), online bulletin, http://www.isc.ac.uk/Bull, 2004, hereinafter referred to as ISC, 2004) event on 4 June 1998 in the Hengill area [*Árnadóttir et al.*, 1999; *Vogfjörd et al.*, 2005], a $M_w = 5.1$ (ISC, 2004) event on 13 November 1998 in the Ölfus area [*Rögnvaldsson et al.*, 1998; *Vogfjörd et al.*, 2005], the 17 June 2000, $M_w = 6.5$ main shock in the SISZ and four $M_w \geq 5$ aftershocks in the SISZ and on the Reykjanes Peninsula [*Vogfjörd*, 2003], the $M_w = 6.5$ main shock on 21 June 2000 in the SISZ, and a $M_w \sim 5$ earthquake on the Reykjanes Peninsula on 23 August 2003 [*Vogfjörd et al.*, 2004]. The data also span a time of increased seismic activity and uplift at the Hengill triple junction between 1993 and 1998 [*Sigmundsson et al.*, 1997; *Feigl et al.*, 2000; *Vogfjörd et al.*, 2005] as well as the February 2000 eruption of Hekla volcano [*Ágústsson et al.*, 2000; *Soosalu et al.*, 2005].

[8] The velocity field during the time interval following the June 2000 earthquake sequence is quite complex due to postseismic deformation [*Árnadóttir et al.*, 2005], and the 2003 earthquake activity on the Reykjanes Peninsula. In this study, we therefore focus on the velocity field in SW Iceland during the preseismic time interval (July 1992 to June 2000), and present kinematic models in an attempt to explain the plate boundary deformation prior to the June 2000 earthquake sequence.

2. Geodetic Data

2.1. GPS Observations

[9] The GPS campaign network in Iceland was first surveyed in 1986 [*Foulger et al.*, 1987]. Since then, the network has been resurveyed many times and densified. GPS measurements have been done on the Reykjanes Peninsula (RP) and the SISZ in 1986, 1989, 1992, 1993 (RP only), 1995 (SISZ only), 1998 (RP only), 1999 (SISZ only), 2000, 2001, 2002, 2003, and 2004 [e.g., *Sigmundsson et al.*, 1995; *Sturkell et al.*, 1994; *Hreinsdóttir et al.*, 2001; *Árnadóttir et al.*, 2001; *Árnadóttir et al.*, 2004]. The quality of the GPS data improved in 1992. The observation sessions are longer, more satellites are available, and the global network of permanent tracking stations is denser. Hence we only use data collected since mid-1992 in our study. Two continuous GPS stations, operated by the IGS [*Beutler et al.*, 1994], in Reykjavík (REYK) and Höfn (HOFN) have been running since 1995 and 1997, respectively. Installation of an Icelandic network of continuous GPS stations (ISGPS) began in March 1999. The details of the continuous GPS network and routine data analysis are described elsewhere (Geirsson et al., submitted manuscript, 2005). We use data from more than 100 GPS campaign stations on the Reykjanes Peninsula and the SISZ from July 1992 to June 2004, as well as all the continuous GPS data available in Iceland through May 2004, to estimate the crustal deformation field in southwest Iceland (Figure 2).

2.2. GPS Data Analysis

[10] We have analyzed all campaign and continuous GPS data collected in southwest Iceland from 1992 to 2004, using the GAMIT/GLOBK software [*King and Bock*, 2003; *Herring et al.*, 1990; *Herring*, 2003]. This approach determines the station position and velocity vectors in a single, self-consistent reference frame, whereas previous studies used different frames for different surveys. This helps mitigate the effects of changes in the network geometry as a function of time.

[11] The data analysis involves two major procedures, as described elsewhere [*Feigl et al.*, 1993; *McClusky et al.*, 2000]. The first procedure uses the GAMIT software to estimate parameters such as station position and orbital trajectory on a daily basis for a given 24-hour interval from the union of three data sets: (1) the campaign stations, (2) the continuously operating GPS stations in Iceland (including the two IGS stations REYK and HOFN), and (3) long-

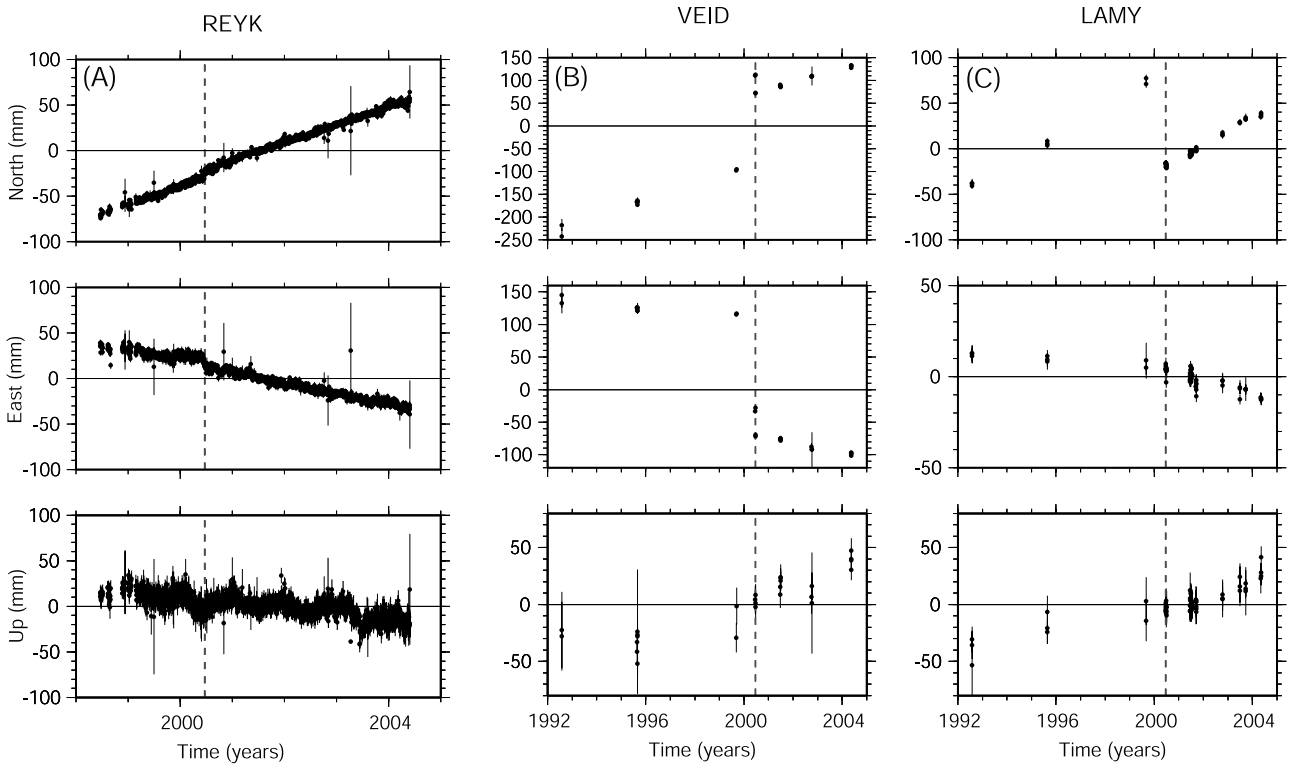

Figure 3. Station positions in the ITRF2000 in east, north, and up, as a function of time. The time of the June 2000 earthquake sequence is shown with a dashed vertical line. Each black dot represents an estimate of the daily station position, and the $1-\sigma$ uncertainties are given by the error bars. (a) Filtered time series of the station position for the continuous station REYK. (b and c) Time series for two campaign stations in the SISZ (VEID and LAMY).

running continuous GPS stations within 5000 km of Iceland (ALGO, MADR, ONSA, TROM, and WES2). The details of the first, daily procedure are completely standard [e.g., *McClusky et al.*, 2000]. The a priori estimates of the satellites' orbital parameters come from the precise trajectories determined by the Scripps Institute of Oceanography (SIO) [*Bock et al.*, 1997] for the surveys before 1994 and from the IGS since then [*Beutler et al.*, 1994].

[12] In the second procedure, we combine the daily solutions with 3 global IGS subnetworks (IGS1, IGS3 and EURO), using the GLOBK software [*Herring*, 2003] in a regional stabilization approach [*McClusky et al.*, 2000]. This stabilization procedure defines a reference frame by minimizing, in the least squares sense, the departure from a priori values based on the International Terrestrial Reference Frame (ITRF) 2000 [*Altamimi et al.*, 2002], of the positions and velocities for a set of 22 well-determined stations in and around Iceland (Table S1, auxiliary material[1]). These stations thus move in a "no net rotation" (NNR) reference frame approximately aligned with the ITRF2000. The misfit to these stabilized stations is 1.8 mm in position and 0.5 mm/yr in velocity, indicating that the uncertainty in the reference frame is of the same order. To decrease the sensitivity of the frame to any errors in the vertical velocities (e.g., satellite antenna phase centers or ionospheric effects), we assign lower weight (larger prior uncertainty) to the vertical velocity estimates by a factor of 10. In the second step of the second procedure, we estimate the positions and velocities of the other stations with respect to the frame defined by the stabilization. For the continuously observing stations, we place a lower bound on their uncertainties by adding 2 mm and 5 mm of white noise to the horizontal and vertical components respectively, to account for the correlation between successive estimates for the station positions.

[13] We parameterize the motion of each station differently according to the relationship in time and space with geophysical events such as earthquakes and eruptions. For example, consider the benchmark at LAMY, that was occupied with GPS in 1992. It was remeasured in 1995, and 1999, as well as several times in the years following the June 2000 earthquake sequence (Figure 3). For this benchmark, we can estimate four three-dimensional vectors, for a total of 12 parameters. The four vectors are the positions of the benchmark and its velocity before and after the June 2000 earthquakes. The coseismic displacements associated with the two June 2000 main shocks are thus the difference between the position vectors after extrapolating the time series to the time of the 17 and 21 June earthquakes, respectively.

[14] Between 1992 and 2004, we define six such events (Table 1). These are the earthquakes on 4 June and 13 November 1998 [*Árnadóttir et al.*, 1999; *Rögnvaldsson et al.*, 1998] the 17 and 21 June 2000 events [*Stefánsson et al.*, 2003], as well as the 23 August 2003 earthquake [*Vogfjörd et al.*, 2004]. The sixth event is the Hekla eruption that

[1]Auxiliary material is available at ftp://ftp.agu.org/apend/jb/2005jb003907.

started on 26 February 2000 [*Ágústsson et al.*, 2000]. At the time of these events, we add additional free parameters (components of position and/or velocity vectors) to describe the motion of benchmarks in the surrounding area. We define the extent of the surrounding area for an epicenter by a radius of influence for each event (Table 1). We arbitrarily chose the same epicentral position for the 17 June earthquakes and the 21 June 2000 main shock to simplify the interpretation. The radius of influence was set to 120 km for these events and 10 km for the others. Unlike the other events parameterized in the time series, the Hengill intrusive episode lasted several years. Accordingly, we will interpret the velocity of the effected stations in this interval, rather than their displacements at its starting time, as the consequences of the inflation.

[15] The availability of data for a given benchmark also determines the parameterization of its motion. To estimate a prequake position requires occupying the station before the earthquake. Similarly, estimating both prequake and postquake velocities requires at least four survey occupations: two before the earthquake and two after. We estimate a velocity for a station if it has at least two occupations separated by at least 0.9 years and there is no earthquake defined during this time interval. These two conditions lead to two relevant cases: (1) If a station has been occupied during two or more campaigns both before and after an earthquake, we can estimate its preseismic and postseismic velocities, as well as a coseismic offset. (2) If, however, a station has only been occupied during a single campaign before an earthquake, its preseismic velocity will not be determined. In this case, however, we can still determine the coseismic displacements, if we assume the preseismic and postseismic velocities to be equal.

3. GPS Velocity Field

[16] The GAMIT/GLOBK solution describes station motions in terms of velocities and displacements in the ITRF2000. The velocities represent the velocity averaged over time, equivalent to the slope of the position time series estimated from the GPS observations. The displacements represent the instantaneous offsets in position estimated at the relevant times. As explained in the introduction, we have several local signals perturbing the overall velocity field in SW Iceland. We therefore divide the time series into intervals, where we assume that the velocity is constant within each interval. We also estimate offsets between the segments at the dates of the events defined in Table 1.

[17] We estimate velocities for stations in the SISZ and on the Reykjanes Peninsula before and after the June 2000 earthquake sequence, as well as a coseismic offset due to the earthquakes on 17 and 21 June 2000. The two time intervals will be referred to as "preseismic" (July 1992 to 17 June 2000) and "postseismic" (21 June 2000 to June 2004) in this paper. Significant postseismic deformation was observed due to the June 2000 earthquake sequence [*Árnadóttir et al.*, 2005]. Since the focus of this study is the broad-scale plate motion we disregard the details of the temporal postseismic velocity variation found in the SISZ and estimate an average velocity for the postseismic time interval. Thus our parameterization of each component of each station's position is a piecewise linear function described by two parameters (offset and slope) per time interval.

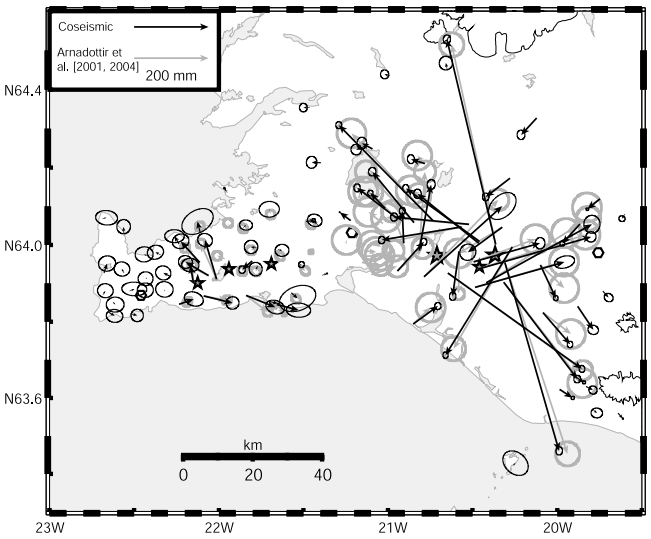

Figure 4. Horizontal coseismic station displacements due to the June 2000 earthquake sequence estimated in this study (black arrows). The gray arrows show the coseismic estimates from previous studies [*Árnadóttir et al.*, 2001; *Árnadóttir et al.*, 2004]. The ellipses denote the 95% confidence limit. The epicentral locations of the two main shocks and four largest triggered events are shown with gray stars.

3.1. Time Series and Coseismic Offsets

[18] The time series for the continuous GPS station REYK and two campaign stations in the SISZ (VEID and LAMY) are shown in Figure 3. The time series for REYK shows two dominant signatures: the linear trend of secular plate motion and seasonal variations, most pronounced in the vertical component. The coseismic offset is less than 10 mm in the horizontal components. Coseismic offsets for the 17 and 21 June 2000 main shocks can be seen at VEID (Figure 3b) because it was one of six campaign stations occupied between the two main shocks. The other five are AKBR, FLAG, HAMR, HJAL, and KOLT. The horizontal offsets are relatively large because the two earthquakes were right-lateral strike-slip events on nearby vertical N-S faults. We also see a postseismic change in velocity following the June 2000 earthquake sequence that is most prominent in the north component at station LAMY (Figure 3c).

[19] The June 2000 earthquake sequence caused significant station displacements in the SISZ and on the Reykjanes Peninsula [*Árnadóttir et al.*, 2001, 2004]. For completeness we estimate the coseismic station displacements in our study area and compare with estimates from the previous studies (Figure 4 and Table S2, auxiliary material). Our solution agrees fairly well with the previous studies considering it is obtained by a different approach, with almost all of the coseismic estimates within the 95% confidence ellipses of the two solutions. The method used in the present study allows us to estimate coseismic offsets at a number of stations that were not included in the previous studies. We also estimate a small coseismic offset at REYK, which was assumed to be fixed previously. The largest discrepancy is

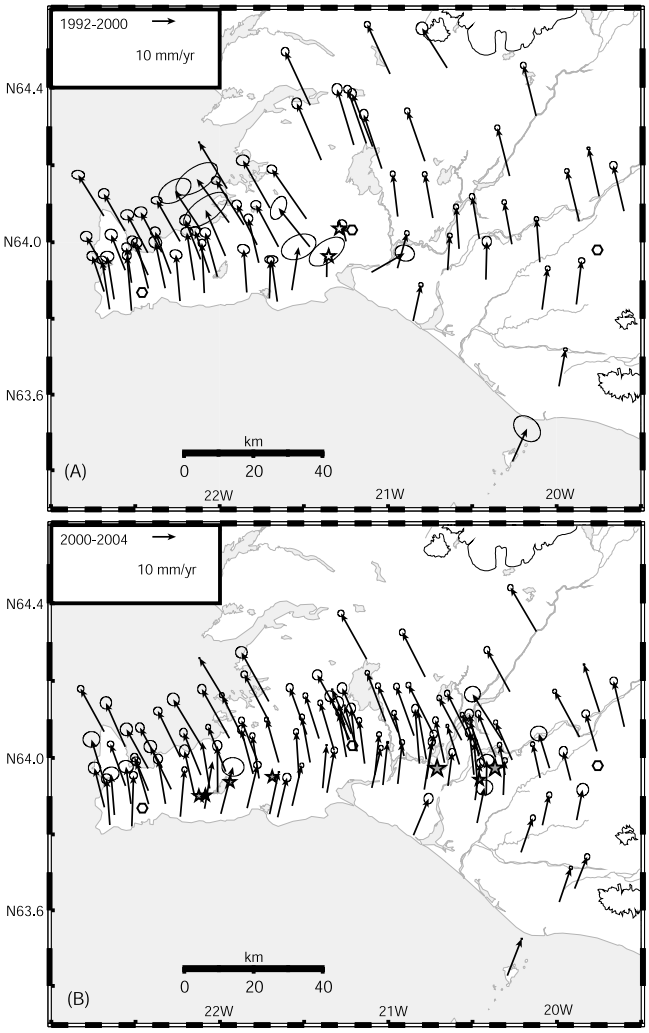

Figure 5. Horizontal station velocities with 95% confidence ellipses in the ITRF2000. (a) The preseismic time interval (July 1992 to June 2000) and (b) the postseismic time interval (June 2000 to June 2004). The stars show epicentral locations of $M_w \geq 5$ earthquakes during the time interval spanned by the GPS data, and hexagons indicate pressure sources.

found at stations near Hengill. The inflation at Hengill (1993–1998) produced significant deformation at stations in the area during the preseismic time interval, compared to the postseismic interval. In addition, many of the stations in this region were affected by the two $M_w \sim 5$ earthquakes in 1998. The campaign GPS stations were not measured frequently enough to separate the effects of inflation at Hengill from 1993 to 1998, the earthquakes in 1998 and the earthquakes in 2000. Accordingly, we estimate only postseismic velocities for most of the campaign stations in the Hengill region.

[20] A $M_w \sim 5$ earthquake occurred on the Reykjanes Peninsula on 23 August 2003 [*Vogfjörd et al.*, 2004] (black star in Figure 2). Horizontal coseismic motion of about 4–5 mm was observed at two nearby GPS campaign stations (SELS and LAMB) [*Vogfjörd et al.*, 2004], but no coseismic offset was observed at VOGS, the closest CGPS station (Geirsson et al., submitted manuscript, 2005). The aftershocks and limited GPS data is consistent with 100 mm of right-lateral strike slip on a 6 km long, N-S vertical fault, extending from about 1.5 km to 5 km depth [*Vogfjörd et al.*, 2004]. The time series for stations within a radius of 10 km of the 23 August earthquake are assumed to have a coseismic break in them. The postseismic velocities for those stations are thus only calculated for the time interval 2000–2003.

3.2. Horizontal Velocity Field

[21] We calculate the surface velocities for the study area before and after the June 2000 earthquake sequence relative to the ITRF2000 (Figure 5). In this reference frame all the stations are moving toward north or northwest. The ITRF2000 is, however, an absolute reference frame with no tectonic significance. We therefore transfer the velocity field into a relative reference frame that better displays the plate boundary deformation. We choose to do this by determining the station velocities relative to stable North America (Figure 6). In this reference frame, stations on the North America plate have small velocities compared to stations on the Eurasia plate. The continuous GPS station VMEY is moving with a velocity that has the same direction but is slightly slower than the predicted REVEL plate motion [*Sella et al.*, 2002] (gray arrow in Figure 6b). The preseismic velocities at stations within a radius of about 25 km from the center of inflation at Hengill are significantly higher than the postseismic velocities, as discussed in section 3.1. There is a significant velocity variation in the SISZ due to postseismic deformation following the June 2000 earthquakes. The details of the postseismic signal have been explained by viscoelastic relaxation assuming a lower crustal viscosity of about 10^{19} Pa s and an upper mantle viscosity of about 3×10^{18} Pa s, and/or afterslip below the main shock ruptures [*Árnadóttir et al.*, 2005]. The preseismic horizontal velocities shown in Figure 6a will be modeled and discussed in more detail in later sections of this paper.

3.3. Vertical Velocity Field

[22] We estimate the vertical velocities for the two time intervals in the same ITRF2000 as described above (Figure 7). We believe this frame is stable to within 1 mm/yr. In this frame, REYK is subsiding at a rate of about 4.0 ± 0.3 mm/yr. Most stations on the Reykjanes Peninsula are subsiding, with higher rates of subsidence along the plate boundary. The broad subsidence signal can only partly be explained by a small rift normal component of the oblique spreading across the peninsula. There are several geothermal areas on the Reykjanes Peninsula, and in one of them, the Svartsengi high-temperature field (labeled Sv in Figure 1), the geothermal exploration is causing localized subsidence. We find a maximum rate of subsidence of 11.0 ± 3.3 mm/yr during 1992–2000, and 9.0 ± 3.5 mm/yr for 2000–2004, relative to REYK, at the station closest to the Svartsengi geothermal power plant (SVAR). This is in good agreement with the rate of subsidence observed by InSAR of 13 mm/yr from 1992 to 1995 [*Vadon and Sigmundsson*, 1997] and 11.2 ± 2.5 mm/yr obtained from GPS measurements from 1993 to 1998 [*Hreinsdóttir et al.*, 2001].

[23] We observe a significant change in vertical velocities between the two time intervals in the Hengill area. Prior to

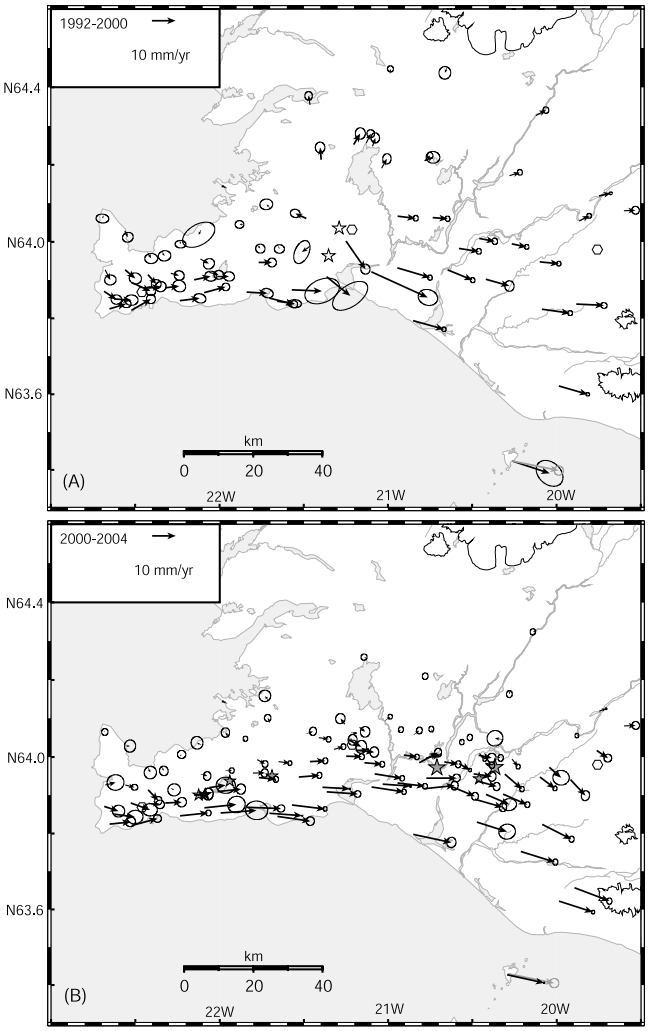

Figure 6. Horizontal station velocities with 95% confidence ellipses, relative to stable North America. (a) The preseismic time interval and (b) the postseismic time interval. The predicted velocity of Eurasia relative to stable North America, from the REVEL plate motion model [*Sella et al.*, 2002], at the location of the campaign site HEIM and the CGPS station VMEY is indicated by a gray arrow. The stars show epicentral locations of $M_w \geq 5$ earthquakes during the time interval spanned by the GPS data, and hexagons indicate pressure sources.

June 2000, previous studies of crustal deformation found uplift in the area, with a maximum rate of 19 mm/yr [*Sigmundsson et al.*, 1997; *Feigl et al.*, 2000]. After June 2000, our GPS velocities show most of the stations subsiding. This is consistent with the termination of the unrest at Hengill at the end of 1998 or early 1999, when seismic activity decreased and uplift observed by GPS ceased [*Hreinsdóttir et al.*, 2001; Geirsson et al., submitted manuscript, 2005]. Most of the stations in the SISZ have upward vertical velocities during both the preseismic and postseismic intervals.

[24] Plotting the rate of vertical velocities along an E-W profile, as a function of longitude (Figure 8), we see a large change in the rate of uplift from the Reykjanes Peninsula in the west, where most stations are subsiding, to the eastern part of the SISZ (~19.5°W) where the stations show uplift at a rate of about 10 mm/yr. The uplift rate decreases to less than 5 mm/yr at the eastern end of the profile (HOFN). A similar rate of uplift is found from an independent analysis of the ISGPS data using the Bernese v4.2 software (Geirsson et al., submitted manuscript, 2005). It is not clear why the uplift rate varies so systematically across southwest Iceland at such a long wavelength. Part of the uplift could be caused by glacial rebound due to the melting of Iceland's largest icecap (Vatnajökull) [*Sigmundsson and Einarsson*, 1992]. Magma accumulation below active volcanoes in the region, such as Hengill and Hekla, could also explain some part of the uplift signal. The subsidence signal on the Reykjanes Peninsula is similarly intriguing. Previous studies [*Hreinsdóttir et al.*, 2001] suggest that this subsidence could be due to lack of magma influx to compensate for the plate spreading. The broad uplift and subsidence observed by GPS in Iceland in this study and others [*Geirsson et al.*, 2005, also submitted manuscript, 2005] could also be a

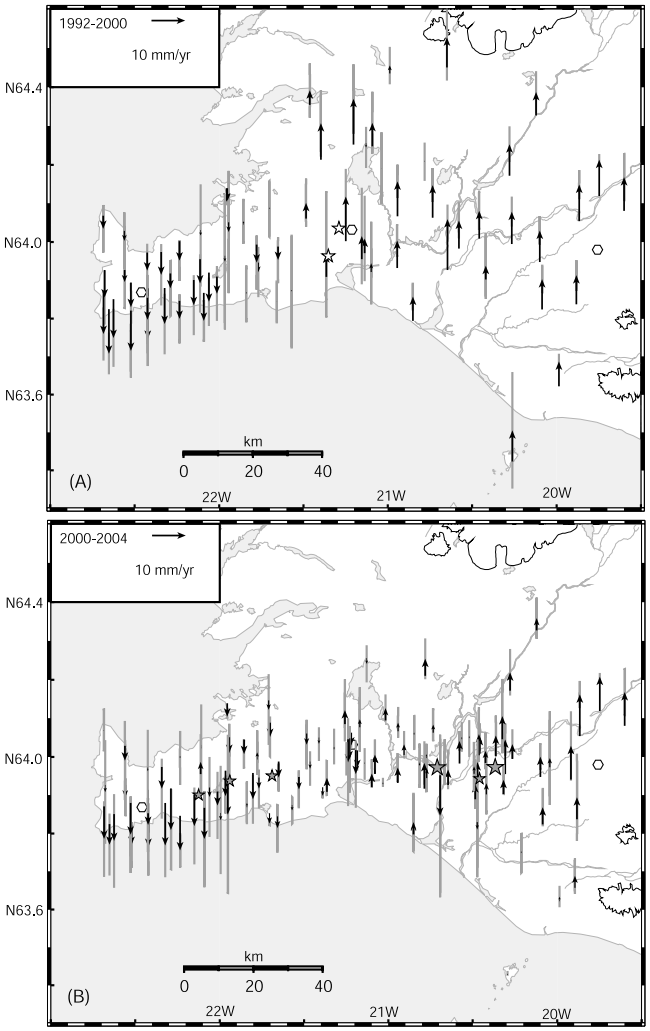

Figure 7. Vertical velocities in the ITRF2000 with 95% confidence limits shown with thick gray bars. (a) The preseismic time interval and (b) the postseismic time interval. The stars show epicentral locations of $M_w \geq 5$ earthquakes during the time interval spanned by the GPS data, and hexagons indicate pressure sources.

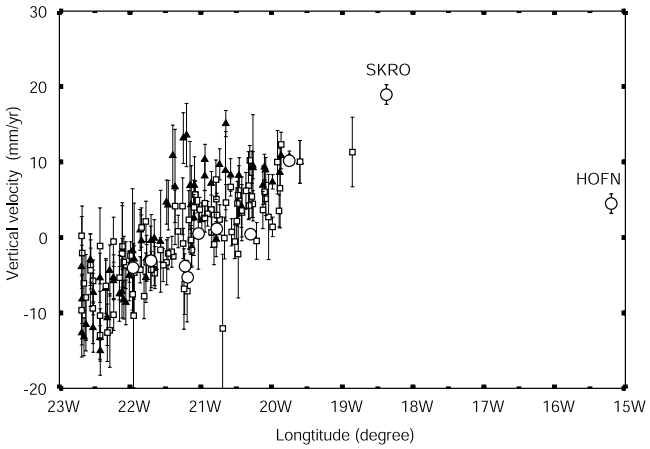

Figure 8. An E-W profile showing the vertical velocity of GPS stations as a function of longitude, from the western tip of the Reykjanes Peninsula (∼23°W) to the IGS station at HOFN (∼15°W). The black triangles are velocities for the preseismic time interval, the open squares are velocities for the postseismic time interval, and circles are velocities at the continuous GPS stations shown in Figure 2.

geodynamic signal from a deep magmatic source, either at the base of the crust or the Icelandic mantle plume. The interpretation of the vertical signal, however, is outside the scope of this study.

4. Plate Boundary Deformation Models

[25] In this section we model the preseismic plate boundary deformation in SW Iceland. We start with a simple screw dislocation model for the Reykjanes Peninsula and the south Iceland seismic zone, assuming that the motion is driven by left-lateral transcurrent motion along the plate boundary, below the brittle-elastic upper crust. In this simple model we assume that the plate boundary is infinitely long, ignoring any opening across the plate boundary and influence from local sources (e.g., Svartsengi and Hengill). We then apply more complex dislocation and point source models to better explain the velocity field in the whole area. In this case we include rift-normal motion along the Western and Eastern volcanic zones, sources of inflation at volcanic centers, deflation at Svartsengi as well as left-lateral motion along the Reykjanes Peninsula and the south Iceland seismic zone. We also test dislocation models where we allow slip on a series of N-S right-lateral strike-slip faults in the south Iceland seismic zone, rather than along a single E-W left-lateral transform.

4.1. Screw Dislocation Models

[26] We first model the preseismic velocity field (Figure 6a) using the simplest model, a screw dislocation in a uniform elastic half space. This model assumes that the brittle crust is locked down to a certain depth and slipping freely below. The velocity v at the surface is then described by [*Savage and Burford*, 1973]

$$v(y) = \frac{V}{\pi}\arctan\left(\frac{y}{D}\right) \tag{1}$$

where y is the distance perpendicular to the plate boundary, D is the locking depth of the crust, and V is the deep slip rate below the locking depth.

[27] We represent the horizontal motion parallel to the plate boundary $v(y)$, as a function of distance y, along a profile perpendicular to the plate boundary, which is located at $y = 0$. We take eastward velocities as positive and the distance along the profile to be positive in northward direction. We seek to explain this profile using equation (1) by searching for optimal values of the locking depth D, deep slip rate V, a shift in the location along the profile δy, and a constant shift in the velocity δv to account for the velocity of North America relative to Eurasia. Equation (1) is therefore slightly modified by replacing $v(y)$ with $\tilde{v}(y) = v(y) + \delta v$ and y with $\tilde{y} = y + \delta y$. We employ a nonlinear optimization scheme that uses a simulated annealing search algorithm, followed by a derivative based method [e.g., *Cervelli et al.*, 2001] to estimate the optimal model parameters, by minimizing the weighted residual sum of squares, $\mathrm{WRSS} = \mathbf{r}^T\Sigma^{-1}\mathbf{r}$. Here $\mathbf{r}$ is the difference between the observed and modeled surface velocities, and Σ is the data covariance matrix.

[28] The model parameters are a nonlinear function of the surface velocity data. We therefore use a bootstrap approach to estimate confidence intervals for our model parameters [*Efron and Tibshirani*, 1986; *Árnadóttir and Segall*, 1994]. The bootstrap method also provides information on correlation of the model parameters. The bootstrap calculation is performed by resampling the original data sets at random with replacement. This means that if the original data set contains N data, we randomly extract N samples, weighted

Table 2. Screw Dislocation Model Parameters Estimated From Preseismic GPS Velocities Relative to Stable North America, Across the Reykjanes Peninsula and the South Iceland Seismic Zone[a]

Region	Time	N	D, km	V, mm/yr	δv, mm/yr	δy, km	χ_ν^2
RNES1	1992–2000	25	4.2	13.7	−5.5	−1.9	2.3
RNES2	1992–2000	22	6.1	15.6	−6.1	−1.0	1.7
RNES[b]	1993–1998	22	6.1	16.0	2.2	0.7	1.1
RNES[c]	1992–2000	22	$6.6^{-4.8}_{+13.2}$	$16.9^{-6.6}_{+20.5}$	$-6.3^{-4.6}_{+2.0}$	$-0.9^{-3.6}_{+6.9}$	
SISZ1	1992–2000	23	13.1	13.4	−10.2	0.7	11.9
SISZ2	1992–2000	20	26.2	19.4	−9.2	−2.9	6.3
SISZ[c]	1992–2000	20	$28.4^{-22.3}_{+36.7}$	$21.5^{-12.4}_{+20.4}$	$-10.0^{-2.0}_{+2.0}$	$1.0^{-10.5}_{+9.1}$	

[a] D is locking depth, V is left-lateral deep slip rate, δv is velocity shift, and δy is shift along profile. The $\chi_\nu^2 = \mathrm{WRSS}/(N - 4)$, where N is the number of data and $m = 4$ is the number of model parameters. Models for Reykjanes Peninsula are labeled with "RNES."Models for the south Iceland seismic zone are labeled with "SISZ."

[b] Velocities from *Hreinsdóttir et al.* [2001].

[c] Mean of 1000 bootstrap models with the 95% lower and upper bounds given.

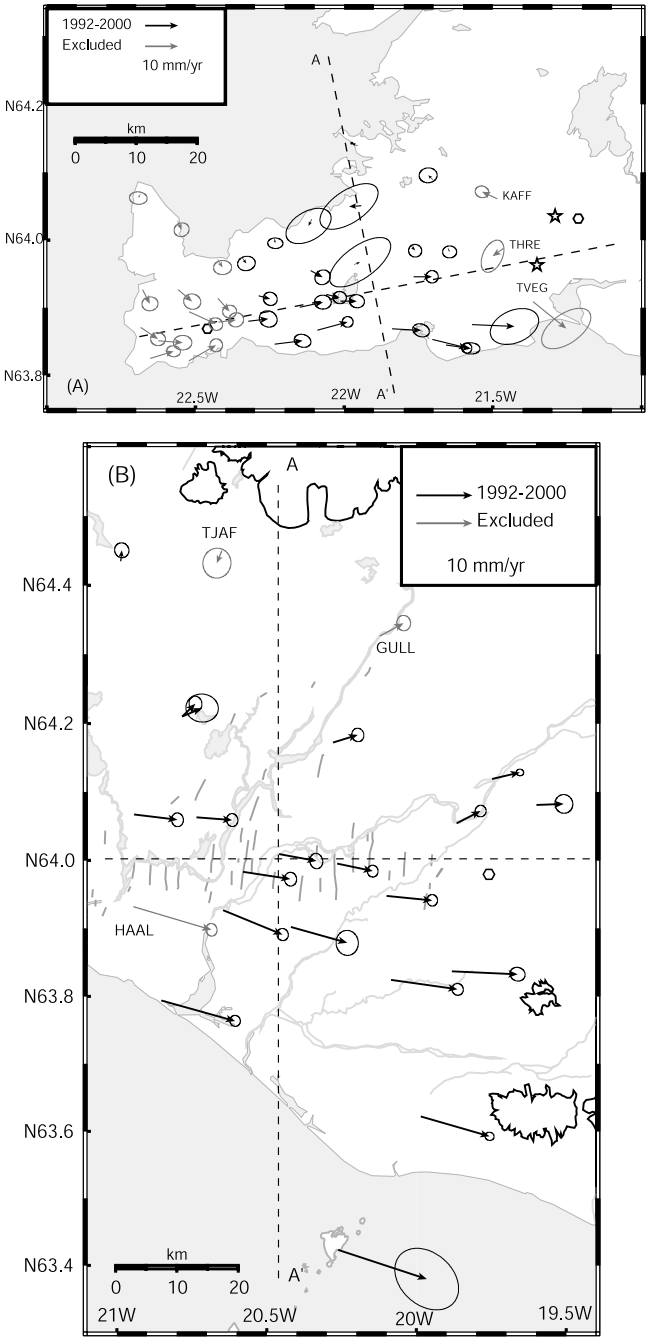

Figure 9. Preseismic velocities of GPS stations used in the screw dislocation models. (a) The Reykjanes Peninsula and (b) the south Iceland seismic zone. Station velocities not used in the inversion are shown with gray arrows. Location of the profile A-A′ is shown with dashed lines in the respective subareas.

by their uncertainties, from the original data set, allowing each datum to be sampled more (or less) than once. We then estimate the optimal model parameters from this resampled weighted data set using our nonlinear inversion algorithm. We perform 1000 bootstrap calculations to estimate a suite of 1000 model parameters. The 95% confidence interval from the bootstrap calculation is estimated using a two-sided bootstrap percentile method [*Efron and Tibshirani*, 1986]. The mean value and the 95% confidence interval for each model parameter are given in Table 2.

4.1.1. Reykjanes Peninsula

[29] We estimate the optimal model parameters assuming a screw dislocation model to explain the preseismic horizontal velocity field in a profile across the Reykjanes Peninsula. The plate boundary appears to bend southward at 22.42°W, with an estimated change in strike from N79°E to N68°E west of 22.42°W. The velocities in the western part of the Reykjanes Peninsula are affected by subsidence at the Svartsengi geothermal field (Figures 6 and 7) rendering a simple screw dislocation model inadequate to fully describe the deformation field over the whole peninsula. We therefore only use velocities from the central and eastern part of the peninsula, between 21.4°W to 22.42°W. We define the origin of our profile at 21.9°W, 63.925°N. The preseismic station velocities used in the screw dislocation modeling, as well as the location of the profile is shown in Figure 9a. The velocity parallel to the plate boundary is shown as a function of the distance along the profile in Figure 10a. The best fit model estimate of the locking depth (D), deep slip rate (V), velocity shift δv and shift in profile origin δy is given in Table 2 and the model fit presented in Figure 10. For the preseismic time interval, we find that excluding three stations (TVEG, THRE and KAFF) that have large residuals and are clearly affected by the inflation at Hengill, significantly improves the fit (models RNES1 and RNES2 in Table 2). The best fit model has a locking depth of 6.1 km and a deep slip rate of 15.6 mm/yr. We also estimate the optimal fault parameters as the mean of 1000 bootstrap calculations (model RNES^c in Table 2) as well and the 95% confidence intervals. The mean of 1000 bootstrap models gives a locking depth of 6.6 km and a deep slip rate of 16.9 mm/yr, similar to the RNES2 solution. The bootstrap 95% confidence intervals we estimate are however quite large, with the locking depth ranging from 2 to 20 km and deep slip rates from 10 to 40 mm/yr, indicating that the model parameters are poorly resolved.

[30] For comparison with *Hreinsdóttir et al.* [2001], we calculate the 4 model parameters using their velocity solution, i.e., assuming a velocity of REYK of 9.19 mm/yr toward west and 0.4 mm/yr south. The optimal model that we find when using their velocities (model RNES^b in Table 2) has V = 16.0 mm/yr, D = 6.1 km, δv = 2.2 mm/yr and δy = 0.7 km. The locking depth and deep slip rates are within the uncertainty given for the optimal solution found by *Hreinsdóttir et al.* [2001], i.e., $V = 16.8 \pm 0.9$ mm/yr and $D = 6.4 \pm 0.8$ km. They estimated a velocity shift of δv = 2 mm/yr, but the origin of their profile is not clearly specified. Our optimal model (RNES2) has a similar locking depth and a deep slip rate as we found using the velocities from *Hreinsdóttir et al.* [2001]. We conclude that the surface velocities parallel to the plate boundary on the Reykjanes Peninsula indicate a locking depth of 6–7 km and a deep slip rate of 16–17 mm/yr, assuming a simple screw dislocation, in agreement with model estimates found by *Hreinsdóttir et al.* [2001]. The model parameters are not well constrained as indicated by the large bootstrap confidence intervals (RNES^c in Table 2).

[31] Scatterplots of 1000 bootstrap estimates clearly show correlations between model parameter pairs (Figure 11a). The density of black dots indicates how well the parameters

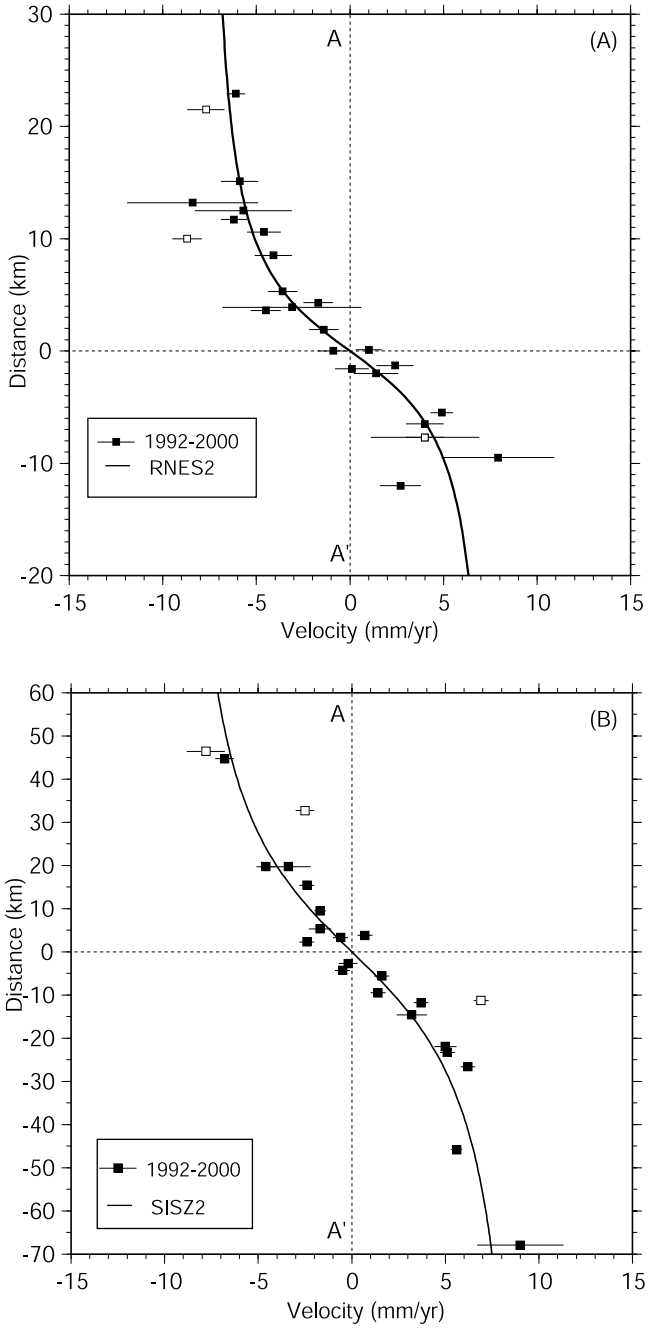

Figure 10. Adjusted preseismic surface velocities parallel to the plate boundary ($\bar{v}(y)$) along profile A-A′ (solid squares) and the velocity profile predicted by the best fit screw dislocation model (solid line). Open squares denote station velocities not included in the inversion. The horizontal lines through the symbols are the 95% confidence limits of the velocities. (a) The Reykjanes Peninsula, east of 22.417°W. The best fit model has a deep slip rate of V = 15.6 mm/yr and a locking depth of D = 6.1 km (RNES2 in Table 2). (b) The south Iceland seismic zone. The solid curve shows model SISZ2 (Table 2) with a deep slip rate of V = 19.4 mm/yr and a locking depth, D = 26.2 km, and the corresponding adjusted data are shown with squares.

are resolved, giving a qualitative distribution of the parameter values. There is a strong trade-off between certain pairs of model parameters, in particular between the deep slip rate V and the locking depth D, as well as between the velocity shift δv and profile shift δy.

4.1.2. South Iceland Seismic Zone

[32] We explore the application of a screw dislocation model to explain the preseismic velocity field across the south Iceland seismic zone (SISZ). We assume that the plate boundary is oriented E-W, and set the origin of our coordinate system at 20.464°W and 64.0°N (Figure 9b). The velocity parallel to the plate boundary is then the east component of the velocity vector.

[33] We use the same method as for the Reykjanes Peninsula to estimate the optimal locking depth D, deep slip rate V, velocity shift δv and shift of the origin δy for the preseismic horizontal velocity field in the SISZ (between 19.87°W and 21°W). We find that excluding data from three stations (HAAL, GULL and TJAF) significantly improves the fit to the data (the χ^2_ν drops from about 12 to 6), but the simple screw dislocation model does not seem to fit the data particularly well since the χ^2_ν is not close to one. Our optimal unconstrained model (model SISZ2 in Table 2) has a locking depth that is quite deep (∼26 km) and a deep slip rate of ∼19 mm/yr. The velocity profile and the optimal model prediction are plotted in Figure 10b. The results from 1000 bootstrap models are given in Table 2 and Figure 11b. The range of possible parameters is quite large for the SISZ with the 95% confidence interval for locking depth ranging from about 6 to 65 km, and deep slip rate from about 9 to 42 mm/yr. It is therefore evident that these parameters are not well resolved by our data if we apply a simple screw dislocation model to the data. As for the Reykjanes Peninsula, the trade-off is particularly strong between the locking depth and the deep slip rate. It therefore appears that we cannot uniquely determine a locking depth and deep slip rate for the SISZ from the preseismic data.

4.2. Dislocation Models of the Plate Boundary

[34] The preseismic GPS velocity field in SW Iceland (Figure 6a) lends itself to a simulation of the plate boundary deformation where several sources contribute to the overall deformation. To construct a more comprehensive model than the simple screw dislocation models, we assume left-lateral motion on vertical dislocations [*Okada*, 1992] along the plate boundary on the Reykjanes Peninsula as well as opening along the Western and Eastern volcanic zones. The plate boundary along the Reykjanes Peninsula is modeled by two dislocations, due to the change in strike from N68°E west of 22.42°W to N79°E east of this location. The strike of the WVZ is set to N30°E and the EVZ has a strike of N48°E. We explore two cases for the SISZ, first a single E-W left-lateral transform, then a series of N-S right-lateral faults. In addition to the dislocations, we include three point sources to model subsidence at the Svartsengi geothermal area, and inflation at Hengill and Hekla volcanoes using the expressions by *Mogi* [1958]. We fix the location and depth of the point sources in Svartsengi, Hengill and Hekla, as well as the rate of volume increase for Hengill based on previous studies [*Feigl et al.*, 2000; *Vadon and Sigmundsson*, 1997]. As explained in section 3.3, the vertical preseismic velocity field has a long-wavelength signal that we cannot fit with this

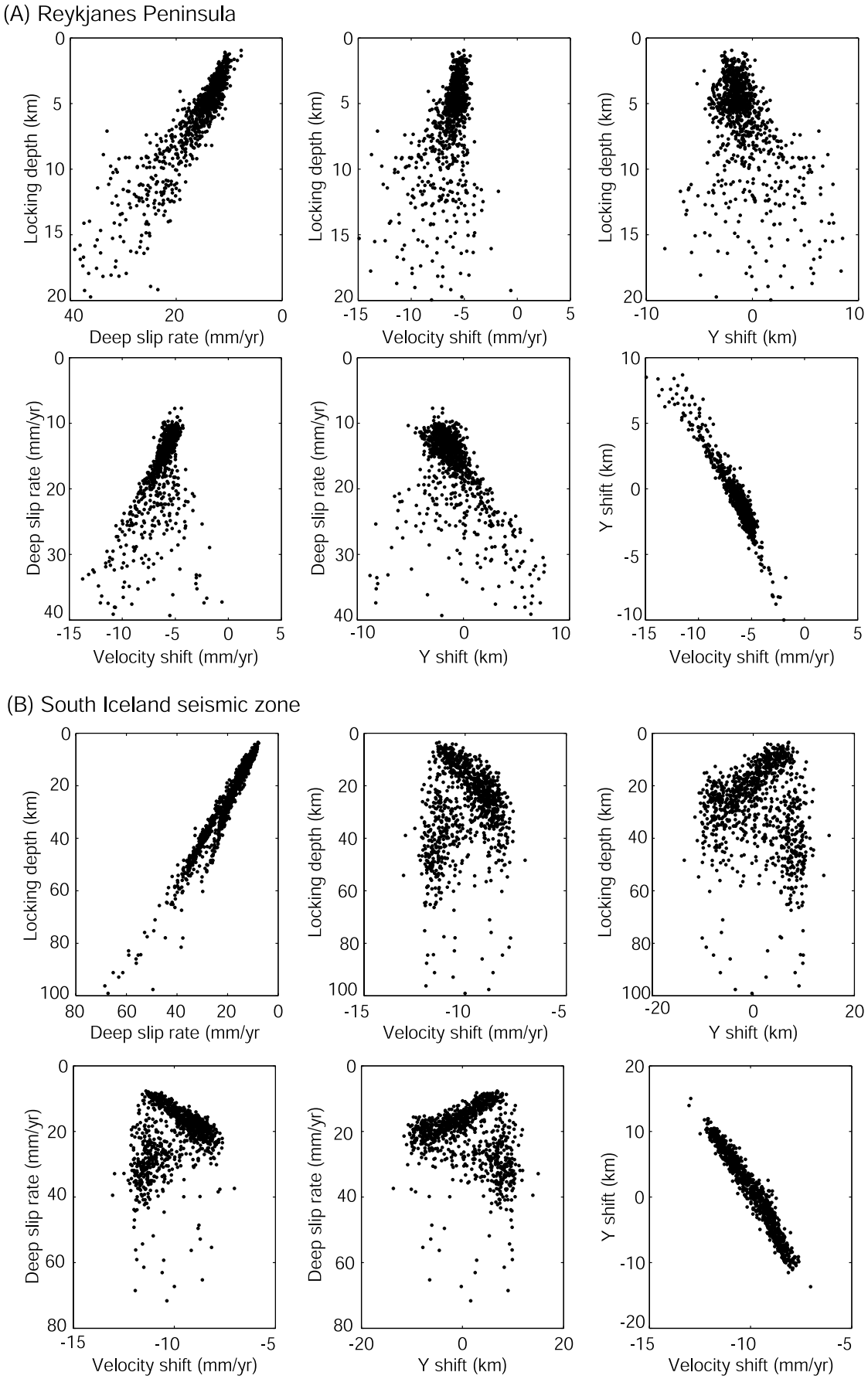
(A) Reykjanes Peninsula
Locking depth (km)
Deep slip rate (mm/yr)
Velocity shift (mm/yr)
Y shift (km)
(B) South Iceland seismic zone

Figure 11

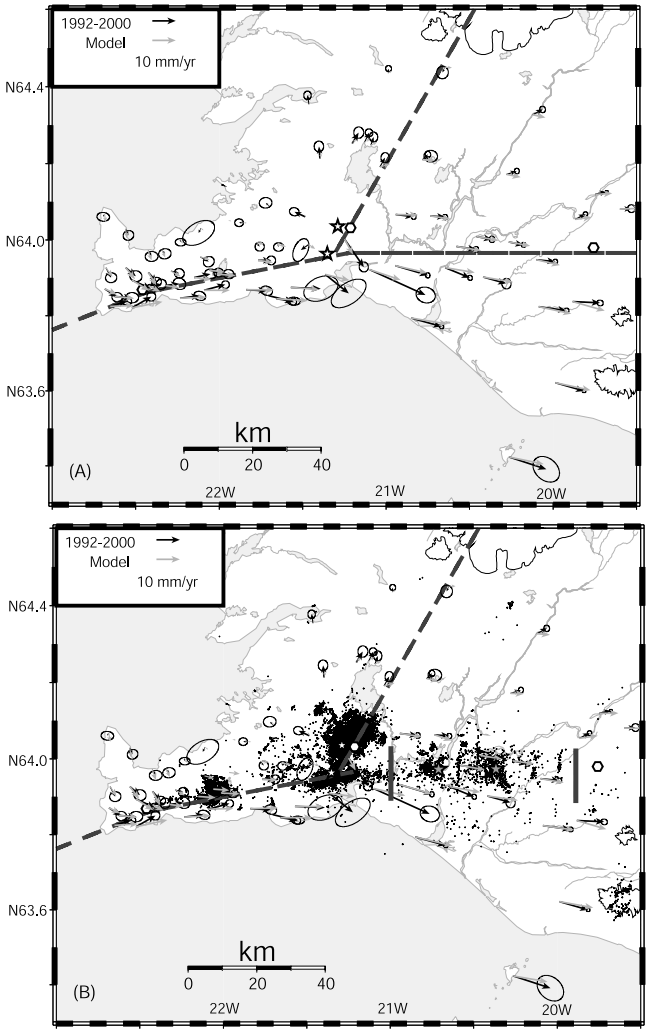

Figure 12. GPS velocities during the preseismic time interval (1992–2000) in SW Iceland (black arrows with 95% confidence ellipses). (a) Predicted velocities (gray arrows) for the optimal plate boundary dislocation and point source model (shown with dashed gray lines and white hexagons) assuming an E-W transform fault for the SISZ. (b) Predicted velocities (gray arrows) for a plate boundary dislocation and point source model (shown with dashed gray lines and white hexagons) assuming deep slip on two N-S faults in the SISZ (bold gray lines). The black crosses show well located, $M \geq 0$ earthquakes from 1992 to 1999, and the stars indicate the locations of the June 2000 main shocks.

simple model. We therefore reduce the importance of the vertical rates by scaling their uncertainties by a factor of 10.

[35] Since we do not have stations spanning the two volcanic zones, we assume a rate of opening of 7 mm/yr and 11 mm/yr below 5 km depth along the Western and Eastern rift zones, respectively, as suggested by *LaFemina et al.* [2005]. We define the length, dip (assumed vertical), strike and location (i.e., a total of 5 parameters) for each dislocation segment of the plate boundary according to geological and/or seismic features. We estimate the remaining model parameters using the nonlinear optimization approach described in section 4.1. We use a total of 65 GPS station velocities, providing 130 horizontal data. If we assume a single E-W transform below the SISZ the total number of model parameters is 62 (i.e., five dislocations with ten parameters each and three point sources with four parameters each). In this case we estimate nine of the 62 model parameters; the rest are fixed. The nine parameters are the locking depths and deep slip rates on the Reykjanes Peninsula (two segments) and the SISZ, opening on the central and eastern part of the Reykjanes Peninsula, and the volume changes of the Svartsengi and Hekla point sources. The observed and predicted horizontal velocities for the best fit model are shown in Figure 12a and the parameters estimated for the optimal model are given in Table 3. This model has a locking depth of about 7 km and 8 km for the western and eastern segments of the Reykjanes Peninsula, respectively. The deep slip rate for the western part of the Reykjanes Peninsula is very fast (about 36 mm/yr), whereas the deep slip rate for the eastern segment is about 17 mm/yr with about 9 mm/yr of opening. The SISZ has a locking depth of about 16 km and a deep slip rate of about 19 mm/yr. The optimal model has a weighted residual sum of squares (WRSS) of 513, and a $\chi^2_\nu = 2.5$. If we do not include a dislocation in the SISZ, the WRSS is about 1100 (the $\chi^2_\nu = 5.2$). The high deep slip rate on the western part of the Reykjanes Peninsula is much higher than velocities predicted by plate motion models. If we constrain the deep slip rate along the western part of the Reykjanes Peninsula to be 20 mm/yr, the optimization algorithm converges on solutions with greater locking depths and higher deep slip rates for the eastern part of the peninsula and the SISZ and the fit is degraded (WRSS = 635 and $\chi^2_\nu = 3.3$). The high deep slip rate we obtain for the western part of the Reykjanes Peninsula appears to be driven by the north trending velocities in the northwestern part of the network. We therefore consider this deep slip rate to be unreliable as it appears to be biased.

[36] We estimate the confidence interval for the free model parameters using the bootstrap method, as explained in section 4.1. The free model parameters are the locking depth and deep slip rates on the Reykjanes Peninsula and the SISZ, and the rate of opening across the eastern part of the Reykjanes Peninsula. The results of the bootstrap calculations are given in Table 3. The mean bootstrap values are comparable to the optimal estimates, and the upper and lower bounds are given as the 95% confidence interval estimated as before. These calculations indicate a shallow locking depth for the western part of the Reykjanes Peninsula, increasing toward east. The deep slip rates for the central and eastern part of the Reykjanes Peninsula and the SISZ range from 17 to 19 mm/yr. More importantly, we find

Figure 11. Scatterplots of 1000 bootstrap estimates of screw dislocation parameters for the preseismic velocities. The density of black dots indicates how well the parameters are resolved giving a qualitative distribution of the parameter values. The plots show a strong trade-off between the deep slip rate and locking depth, as well as the velocity shift and profile location. (a) The Reykjanes Peninsula and (b) the south Iceland seismic zone.

Table 3. Dislocation Model Parameters[a]

Model	D_{RPW}, km	V_{RPW}, mm/yr	D_{RP}, km	V_{RP}, mm/yr	OP_{RP}, mm/yr	D_{SISZ}, km	V_{SISZ}, mm/yr
Optimal	6.6	35.9	8.3	17.4	8.9	15.6	19.3
Mean	6.3	35.2	8.6	18.0	9.0	14.7	19.1
Lower	4.6	33.0	5.9	13.0	6.3	5.4	9.5
Upper	8.0	38.4	11.7	24.1	12.2	22.7	28.8

[a]D is the locking depth, V is the deep slip rate assuming left-lateral slip and OP is the rate of opening. The subscripts on the model parameters indicate the sections of the plate boundary, i.e., RPW is the western part of the Reykjanes Peninsula, RP is the central and eastern part of the Reykjanes Peninsula, and SISZ is the south Iceland seismic zone. The locking depth and rate of opening are fixed at 5 km and 7 mm/yr for the WVZ and 5 km and 11 mm/yr for the EVZ. The optimal model is obtained using all the data, whereas the "mean" denotes the mean values for the model parameters estimated from 1000 bootstrap models, and "lower" and "upper" are the 95% confidence limits for the lower and upper bounds of the bootstrap models, respectively.

a component of opening of about 9 mm/yr across the central and eastern part of the Reykjanes Peninsula, which has not been obtained from previous studies [*Hreinsdóttir et al.*, 2001].

[37] In the second suite of models we assume that the interseismic deformation is driven by deep slip on N-S faults in the SISZ, rather than on a single E-W transform. The N-S faults are assumed to be 10–15 km long, vertical, with right-lateral strike slip below a locking depth estimated by the optimization algorithm. We find that the fit to the data improves considerably when we increase the number of N-S faults in the SISZ from one to two (WRSS = 601 and a $\chi^2_\nu = 2.9$ for one dislocation compared to WRSS = 518 and a $\chi^2_\nu = 2.6$ for two), but remains similar for two to five dislocations (WRSS $\sim$ 500 and a $\chi^2_\nu \sim 2.6$). The two-fault optimal model places the dislocations in the western and eastern part of the SISZ, neither one in an area with background seismicity (Figure 12b). The westernmost structure has a fairly shallow locking depth for all five cases (5–8 km) and a fast deep slip rate of about 40 mm/yr, probably due to the fast velocities of two stations east of Hengill. The eastern structure has a deeper locking depth (17–20 km) and an even faster deep slip rate of about 80 mm/yr. In models with two or more faults the western and eastern most structures appear fairly consistent in location, locking depth and deep slip rate, whereas the other faults are located in the central part of the SISZ with locking depths ranging from 30 to 45 km, and deep slip rates ranging from 2 to 70 mm/yr. The data therefore do not indicate slip below the June 17 and 21, 2000 ruptures (above 20 km) prior to the earthquakes there.

[38] From the above calculations, we conclude that slip on N-S faults at shallow depths (5–15 km) in the SISZ is not supported by the preseismic GPS velocities. Instead, a simple E-W shear zone below 15–20 km depth is a more plausible model for the interseismic deformation in the SISZ, as it is unreasonable to expect slip below 30 km depth on N-S structures that are 10–15 km long, and the deep slip rates we obtained for the N-S structures appear very high.

[39] The estimated volume change for the Hekla magma source, assuming a source depth of 10 km, is about 0.0037 km^3/yr. This rate appears reasonable during the period of inflation (1992–2000), but is not well constrained by our data. If we do not constrain the volume change for Hengill, we find a rate of inflation of about 0.007 km^3/yr for a source depth of 7 km, which is considerably higher than estimated from InSAR data [*Feigl et al.*, 2000]. This large rate of volume change is partly due to high velocities at two stations located east of Hengill. As explained in sections 1–3, the preseismic velocities are difficult to determine in the Hengill area due to the two $M \sim 5$ earthquakes in 1998. We therefore constrain the volume change for the Hengill source, as explained above, to 0.0039 km^3/yr, the rate obtained from the InSAR study [*Feigl et al.*, 2000].

5. Discussion

[40] In this study we present a surface velocity map for SW Iceland derived from GPS data. We explore a range of models in order to explain the horizontal GPS velocity field, focusing on the preseismic time interval from July 1992 to June 2000. First we apply simple screw dislocation models, and find a large range of locking depths and slip rates that can fit the horizontal velocity field on the Reykjanes Peninsula and the SISZ. For the Reykjanes Peninsula the bootstrap models give a mean locking depth of 7 km and a mean deep slip rate of 17 mm/yr. It is likely that the inflation at Hengill affects our model results for the Reykjanes Peninsula, as well as the assumption that the plate boundary can be approximated by an infinitely long screw dislocation. For the SISZ there is a strong trade-off between the deep slip rate and locking depths that we are unable to resolve. For a reasonable deep slip rate ($\sim$20 mm/yr) we obtain a locking depth of $\sim$25 km for the SISZ.

[41] Simple screw dislocation models are inadequate to explain the velocity field in SW Iceland, as they account neither for local deformation due to volcanoes nor the spreading across the rift zones. Furthermore, in applying a screw dislocation we assume that the plate boundary is infinitely long. We therefore test more complex models, consisting of several dislocations and point sources. Since the data do not constrain all the model parameters, we fix many of them based on results from several independent deformation studies. As with the screw dislocation models, we find a trade-off between the deep slip rate and locking depth such that a higher deep slip rate results in a greater locking depth. There is a large uncertainty in our model estimates that is difficult to quantify because of the trade-off among the parameters for the different sections of the plate boundary. For example, fixing the deep slip rate on the western part of the Reykjanes Peninsula influences the parameters for the other dislocations. We test two fault model geometries for the SISZ: an E-W transform and series of N-S faults. Assuming an E-W left-lateral shear zone below the SISZ gives a similar fit to the data as assuming

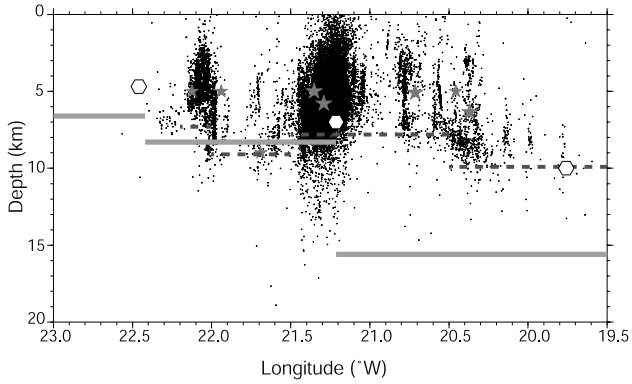

Figure 13. An E-W cross section of well-located $M \geq 0$ earthquakes from 1992 to 1999 (black crosses), located between N63.85° and N64.15°, showing the hypocenter depths as a function of longitude in SW Iceland. The gray stars are $M \geq 5$ earthquakes in 1998 and June 2000. The hexagons show the locations of the Mogi point sources described in the text. The thick gray lines indicate the locking depths from the optimal plate boundary dislocation model. The dashed lines show the estimated thickness of the seismogenic crust (D_{95}).

two or more N-S faults. The simplest models for the SISZ are therefore an E-W left-lateral transform slipping at about 19 mm/yr below about 16 km depth, or two N-S faults with the western fault slipping at 40 mm/yr below 8 km depth and the eastern fault slipping at 97 mm/yr below 18 km depth. We prefer the simpler model of an E-W transform below the SISZ as explained in the previous section, although we cannot rule out alternative models of slip on deep N-S faults. For our preferred model of the SISZ, we find locking depths of about 7 km in the western part of the Reykjanes Peninsula, and about 8 km for the central and eastern part of the peninsula, with a deep slip rate of about 36 mm/yr and 17 mm/yr for the western and eastern parts, respectively. A previous study using GPS data from the Reykjanes Peninsula found a locking depth of about 6.5 km and a deep slip rate of 16.5 mm/yr, assuming a simple screw dislocation model [*Hreinsdóttir et al.*, 2001]. It concluded that there was no significant opening across the Reykjanes Peninsula. We, however, estimate about 9 mm/yr of opening across the central and eastern part of the Reykjanes Peninsula. The rather simple optimal plate boundary model we obtain can explain the first-order features of the velocity field in SW Iceland.

[42] To explore the implications of our modeling, we attempt to interpret them in terms of rheology. The maximum depth of earthquakes is an indication of the transition from brittle fracture to ductile flow [e.g., *Sibson*, 1982, 1986; *Scholz*, 1990]. The thickness of the brittle crust is often defined as the depth above which 95% of the earthquakes occur (D_{95}). Figures 12b and 13 show a map view and an E-W cross section of well located earthquakes (location error less than about 2 km) in our study area from 1992 to 1999. There are several areas of high seismic activity, in particular the Hengill area. The E-W cross section shows that most of the seismicity is located above ~10 km depth. The thickness of the seismogenic crust can be estimated by calculating the D_{95} for several sections from east to west. We find that the thickness of the seismogenic layer is ~10 km from 19.5° W to 20.5°W, where it decreases to about 8 km thickness west to about 21.5°W. There the thickness increases again to ~9 km, in the area from 21.5°W to 22°W, decreasing to ~7 km again farther west. The earthquakes in the western part of the SISZ are shallower than in the eastern part, as suggested in previous studies [*Einarsson*, 1991; *Stefánsson et al.*, 1993]. The earthquake hypocenters on the Reykjanes Peninsula cluster in discrete areas, reaching down to 7–9 km depth, similar to what is observed in the SISZ. Our estimates are in general agreement with the depth to the base of the brittle curst obtained from relocated earthquakes in a three-dimensional (3-D) tomographic study by *Tryggvason et al.* [2002]. Figure 13, however, clearly demonstrates that the seismicity on the Reykjanes Peninsula is not significantly shallower than in the SISZ. Our optimal model suggests a locking depth of about 8 km for the central and eastern part of the Reykjanes Peninsula, which is comparable to the maximum depth of seismicity. A locking depth of about 15 km for the SISZ is significantly deeper than most of the hypocenter depths during this time interval. Half-space models tend to underestimate the source depth compared to 1-D velocity models used for estimating earthquake hypocenter locations, but the bias is unlikely to exceed 1 km [*Cattin et al.*, 1999; *Hooper et al.*, 2002]. The discrepancy we find between the locking depth and the thickness of the seismogenic crust in the SISZ cannot be explained by our assumption of a homogenous half-space, rather than a layered medium, the locking depth is greater than the thickness of the seismogenic crust. Our dislocation models assume that the deep slip rate changes abruptly from zero above the locking depth to a constant value below, in discrete segments along the plate boundary. The brittle-ductile transition, however, does not occur sharply at a fixed depth, because it depends on several parameters, such as the strain rate, fluid pressure, temperature, and rock composition, [e.g., *Sibson*, 1986; *Tse and Rice*, 1986; *Scholz*, 1990]. Such a gradual transition from "locked" to "unlocked" over a range of several km in depth would likely overlap with a similarly gradual transition from "brittle" to "ductile" as defined by the seismicity. It is therefore possible that models that allow a gradual increase of slip with depth, as well as a variation in locking depth along strike, would show a better agreement with the depth of seismicity in the SISZ. Resolving such details, however, requires better spatial data coverage than is provided by the available preseismic GPS data. Given the simplicity of our model and the uncertainties in the earthquake hypocenter depths, we therefore conclude that the estimated locking depths are in general agreement with the estimated thickness of the seismogenic layer on the Reykjanes Peninsula. In the SISZ, however the best fit locking depth is significantly deeper than our estimate of the thickness of the seismogenic layer.

6. Conclusions

[43] We present a consistent surface velocity map for the Reykjanes Peninsula and the south Iceland seismic zone derived from GPS data collected between 1992 and 2004. The surface velocities are estimated for two time intervals: a preseismic velocity field from July 1992 to 17 June 2000

and a postseismic field from 21 June 2000 to May 2004, using repeated GPS campaign and continuous measurements. We also estimate coseismic displacements in the SISZ and on the Reykjanes Peninsula, due to the June 2000 earthquake sequence. In this study we focus on the preseismic GPS velocity field in SW Iceland. Our preferred model of the plate boundary consists of several elastic dislocations and point sources. On the central and eastern part of the Reykjanes Peninsula, the locking depth is about 8 km with left-lateral deep slip rate of about 17 mm/yr, and about 9 mm/yr of opening. In the SISZ the locking depth is about 16 km with a deep slip rate of 19 mm/yr along an E-W left-lateral transform. The locking depth agrees reasonably well with estimates of the thickness of the seismogenic crust for the Reykjanes Peninsula (7–9 km) but is significantly deeper below the SISZ. We suggest that the SISZ is a complex zone with N-S faulting observed at the surface driven by E-W left-lateral shear below 15–20 km depth.

[44] **Acknowledgments.** We thank everyone who participated in collecting the vast amount of GPS data used in this study. B. Thorbjarnardóttir at the Icelandic Meteorological Office provided the hypocenter locations shown in Figure 13. We are grateful to Sigrún Hreinsdóttir, Páll Einarsson, Fred Pollitz, Tim Dixon, Jim Savage, Freysteinn Sigmundsson, Amy Clifton, and Pete LaFemina for discussions and comments. Comments from two anonymous reviewers helped us improve this manuscript. This work was supported in part by grants from the University of Iceland Research Fund (P. Einarsson, early GPS surveys), Icelandic Research Council grant 031590003, EU contract EVG1-CT-2001-0044 (RETINA), and EU contract EVG1-CT-2002-00073 (PREPARED). Most of the figures were produced using the GMT public domain software [*Wessel and Smith*, 1998].

References

Ágústsson, K., R. Stefánsson, A. T. Linde, P. Einarsson, I. S. Sacks, G. B. Gudmundsson, and B. Thorbjarnardóttir (2000), Successful prediction and warning of the 2000 eruption of Hekla based on seismicity and strain changes, *Eos Trans. AGU*, *81*(48), Fall Meet. Suppl., Abstract V11B-30.

Altamimi, Z., P. Sillard, and C. Boucher (2002), ITRF2000: A new release of the International Terrestrial Reference Frame for earth science applications, *J. Geophys. Res.*, *107*(B10), 2214, doi:10.1029/2001JB000561.

Antonioli, A., M. E. Belardinelli, A. Bizzarri, and K. S. Vogfjörd (2006), Evidences of instantaneous dynamic triggering during the seismic sequence of year 2000 in South Iceland, *J. Geophys. Res.*, *111*, B03302, doi:10.1029/2005JB003935.

Árnadóttir, T., and P. Segall (1994), The 1989 Loma Prieta earthquake imaged from inversion of geodetic data, *J. Geophys. Res.*, *99*, 21,835–21,855.

Árnadóttir, T., S. Rögnvaldsson, K. Ágústsson, R. Stefánsson, S. Hreinsdóttir, K. Vogfjörd, and G. Thorbergsson (1999), Seismic swarms and surface deformation in the Hengill area, SW Iceland, *Seismol. Res. Lett.*, *70*, 269.

Árnadóttir, T., H. Geirsson, B. H. Bergsson, and C. Völksen (2000), The Icelandic continuous GPS network— ISGPS, March 18, 1999–February 20, 2000, *Rep. VI-R00002-JA02*, 36 pp., Icelandic Meteorol. Off., Reykjavík, Iceland.

Árnadóttir, T., S. Hreinsdóttir, G. Gudmundsson, P. Einarsson, M. Heinert, and C. Völksen (2001), Crustal deformation measured by GPS in the south Iceland seismic zone due to two large earthquakes in June 2000, *Geophys. Res. Lett.*, *28*, 4031–4033.

Árnadóttir, T., H. Geirsson, and P. Einarsson (2004), Coseismic stress changes and crustal deformation on the Reykjanes Peninsula due to triggered earthquakes on 17 June 2000 (2004), *J. Geophys. Res.*, *109*, B09307, doi:10.1029/2004JB003130.

Árnadóttir, T., S. Jónsson, F. F. Pollitz, W. Jiang, and K. L. Feigl (2005), Postseismic deformation following the June 2000 earthquake sequence in the south Iceland seismic zone, *J. Geophys. Res.*, *110*, B12308, doi:10.1029/2005JB003701.

Beutler, G., I. I. Mueller, and R. E. Neilan (1994), The International GPS Service for Geodynamics: Development and start of official service on January 1, 1994, *Bull. Geod.*, *68*, 39–70.

Bock, Y., et al. (1997), Southern California Permanent GPS Geodetic Array: Continuous measurements of regional crustal deformation between the 1992 Landers and 1994 Northridge earthquakes, *J. Geophys. Res.*, *102*, 18,013–18,033.

Cattin, R., P. Briole, H. Lyon-Caen, P. Bernard, and P. Pinettes (1999), Effects of superficial layers on coseismic displacements for a dip-slip fault and geophysical implications, *Geophys. J. Int.*, *137*, 149–158.

Cervelli, P., M. H. Murray, and P. Segall (2001), Estimating source parameters from deformation data, with an application to the March 1997 earthquake swarm off the Izu Peninsula, Japan, *J. Geophys. Res.*, *106*, 11,217–11,237.

Clifton, A. E., and P. Einarsson (2005), Styles of surface rupture analysis accompanying the June 17 and 21, 2000 earthquakes in the south Iceland seismic zone, *Tectonophysics*, *396*, 141–159.

Clifton, A. E., C. Pagli, J. F. Jónsdóttir, K. Eythórsdóttir, and K. Vogfjörd (2003), Surface effects of triggered fault slip on Reykjanes Peninsula, SW Iceland, *Tectonophysics*, *369*, 145–154.

DeMets, C. G., R. G. Gordon, D. F. Argus, and S. Stein (1990), Current plate motions, *Geophys. J. Int.*, *101*, 425–478.

DeMets, C. G., R. G. Gordon, D. F. Argus, and S. Stein (1994), Effect of recent revisions to the geomagnetic reversal time scale on estimates of current plate motions, *Geophys. Res. Lett.*, *21*, 2191–2194.

Efron, B., and R. Tibshirani (1986), Bootstrap methods for standard errors, confidence intervals, and other measures of statistical accuracy, *Stat. Sci.*, *1*, 54–77.

Einarsson, P. (1991), Earthquakes and present-day tectonism in Iceland, *Tectonophysics*, *189*, 261–279.

Einarsson, P., and J. Eiríksson (1982), Earthquake fractures in the districts Land and Rangárvellir in the south Iceland seismic zone, *Jökull*, *32*, 113–120.

Einarsson, P., and K. Smundsson (1987), Earthquake epicenters 1982–1985 and volcanic systems in Iceland, in *Í hlutarins edli, Map accompanying festschrift for T. Sigurgeirsson*, edited by T. I. Sigfusson, Menningarsjodur, Reykjavík, Iceland.

Einarsson, P., S. Björnsson, G. Foulger, R. Stefánsson, and T. Skaftadóttir (1981), Seismicity pattern in the south Iceland seismic zone, in *Earthquake Prediction: An International Review*, *Maurice Ewing Ser.*, vol. 4, edited by D. W. Simpson and P. G. Richards, pp. 141–151, AGU, Washington, D. C.

Feigl, K. L., et al. (1993), Space geodetic measurement of crustal deformation in central and southern California, 1984–1992, *J. Geophys. Res.*, *98*, 21,677–21,712.

Feigl, K. L., J. Gasperi, F. Sigmundsson, and A. Rigo (2000), Crustal deformation near Hengill volcano, Iceland 1993–1998: Coupling between magmatic activity and faulting inferred from elastic modeling of satellite radar interferograms, *J. Geophys. Res.*, *105*, 25,655–25,670.

Foulger, G. R., R. Bilham, W. J. Morgan, and P. Einarsson (1987), The Icelandic GPS geodetic field campaign 1986, *Eos Trans. AGU*, *68*, 1809.

Geirsson, H., T. Árnadóttir, E. Sturkell, W. Jiang, M. Rennen, C. Völksen, C. Pagli, T. Sigurdsson, T. Theodorsson, J. Erlingsson, P. Einarsson, and F. Sigmundsson (2005), Crustal deformation in Iceland derived from the nation-wide 1993 and 2004 ISNET campaigns, *Eos Trans. AGU*, *86*(52), Fall Meet. Suppl., Abstract G21B-1275.

Hackman, M. C., G. C. P. King, and R. Bilham (1990), The mechanics of the south Iceland seismic zone, *J. Geophys. Res.*, *95*, 17,339–17,351.

Herring, T. A. (2003), GLOBK: Global Kalman filter VLBI and GPS analysis program version 4.1, Mass. Inst. of Technol., Cambridge.

Herring, T. A., J. L. Davis, and I. I. Shapiro (1990), Geodesy by radio interferometry: The application of Kalman filtering to very long baseline interferometry data, *J. Geophys. Res.*, *95*, 12,561–12,581.

Hooper, A., P. Segall, K. Johnson, and J. Rubinstein (2002), Reconciling seismic and geodetic models of the 1989 Kilauea south flank earthquake, *Geophys. Res. Lett.*, *29*(22), 2062, doi:10.1029/2002GL016156.

Hjaltadóttir, S., K. S. Vogfjörd, and R. Slunga (2005), Mapping subsurface faults in southwest Iceland using relatively located microearthquakes, *Geophys. Res. Abstr.*, *7*, Abstract EGU05-A-06664.

Hreinsdóttir, S., P. Einarsson, and F. Sigmundsson (2001), Crustal deformation at the oblique spreading Reykjanes Peninsula, SW Iceland: GPS measurements from 1993 to 1998, *J. Geophys. Res.*, *106*, 13,803–13,816.

Jóhannesson, H., S. P. Jakobsson, and K. Sæmundsson (1990), Geolocial map of Iceland, sheet 6, south Iceland, 3rd ed., Icelandic Mus. Nat. Hist. and Icelandic Geod. Surv., Reykjavík.

King, R. W., and Y. Bock (2003), Documentation for the GAMIT Analysis Software release 10.1, Mass. Inst. Technol., Cambridge.

LaFemina, P. C., T. H. Dixon, R. Malservisi, T. Árnadóttir, E. Sturkell, F. Sigmundsson, and P. Einarsson (2005), Geodetic GPS measurements in south Iceland: Strain accumulation and partitioning in a propagating ridge system, *J. Geophys. Res.*, *110*, B11405, doi:10.1029/2005JB003675.

McClusky, S., et al. (2000), Global Positioning System constraints on plate kinematics and dynamics in the eastern Mediterranean and Caucasus, *J. Geophys. Res.*, *105*, 5695–5720.

Mogi, K. (1958), Relations between the eruptions of various volcanoes and the deformation of the ground surfaces around them, *Bull. Earthquake Res. Inst. Univ. Tokyo*, *36*, 99–134.

Okada, Y. (1992), Internal deformation due to shear and tensile faults in a half-space, *Bull. Seismol. Soc. Am.*, *82*, 1018–1040.

Pagli, C., R. Pedersen, F. Sigmundsson, and K. L. Feigl (2003), Triggered seismicity on June 17, 2000 on Reykjanes Peninsula, SW-Iceland captured by radar interferometry, *Geophys. Res. Lett.*, *30*(6), 1273, doi:10.1029/2002GL015310.

Pedersen, R., F. Sigmundsson, K. L. Feigl, and T. Árnadóttir (2001), Coseismic interferograms of two M_S = 6.6 earthquakes in the south Iceland seismic zone, June 2000, *Geophys. Res. Lett.*, *28*, 3341–3344.

Pedersen, R., S. Jónsson, T. Árnadóttir, F. Sigmundsson, and K. L. Feigl (2003), Fault slip distribution of two M_w = 6.5 earthquakes in south Iceland estimated from joint inversion of InSAR and GPS measurements, *Earth Planet. Sci. Lett.*, *213*, 487–502.

Rögnvaldsson, S. T., et al. (1998), An earthquake sequence in Ölfus in November 1998 (in Icelandic), *Rep. VI-G98046-JA09*, Icelandic Meteorol. Off., Reykjavík.

Savage, J. C., and R. O. Burford (1973), Geodetic determination of relative plate motion in central California, *J. Geophys. Res.*, *78*, 832–845.

Scholz, C. H. (1990), *The Mechanics of Earthquakes and Faulting*, 439 pp, Cambridge Univ. Press, New York.

Sibson, R. H. (1982), Fault zone models, heat flow, and the depth distribution of earthquakes in the continental crust of the continental United States, *Bull. Seismol. Soc. Am.*, *72*, 151–163.

Sibson, R. H. (1986), Earthquakes and rock deformation in crustal fault zone, *Annu. Rev. Earth Planet. Sci.*, *14*, 149–175.

Sella, G. F., T. H. Dixon, and A. Mao (2002), REVEL: A model for Recent plate velocities from space geodesy, *J. Geophys. Res.*, *107*(B4), 2081, doi:10.1029/2000JB000033.

Sigmundsson, F., and P. Einarsson (1992), Glacio-isostatic crustal movements caused by historical volume change of the Vatnajökull ice cap, Iceland, *Geophys. Res. Lett.*, *19*(21), 2123–2126.

Sigmundsson, F., P. Einarsson, and R. Bilham (1992), Magma chamber deflation recorded by the Global Positioning System: The Hekla 1991 eruption, *Geophys. Res. Lett.*, *19*(14), 1483–1486.

Sigmundsson, F., P. Einarsson, R. Bilham, and E. Sturkell (1995), Rift-transform kinematics in south Iceland: Deformation from Global Positioning System measurements, 1986 and 1992, *J. Geophys. Res.*, *100*, 6235–6248.

Sigmundsson, F., P. Einarsson, S. T. Rögnvaldsson, G. R. Foulger, K. M. Hodgkinsson, and G. Thorbergsson (1997), The 1994–1995 seismicity and deformation at the Hengill triple junction, Iceland: Triggering of earthquakes by minor magma injection in a zone of horizontal shear stress, *J. Geophys. Res.*, *102*, 15,151–15,161.

Soosalu, H., P. Einarsson, and B. Thorbjarnardóttir (2005), Seismic activity associated with the 2000 eruption of Hekla, Iceland, *Bull. Volcanol.*, *68*, 21–36, doi:10.1007/s00445-005-0417-7.

Stefánsson, R., R. Bödvarsson, R. Slunga, P. Einarsson, S. Jakobsdóttir, H. Bungum, S. Gregersen, J. Havskov, J. Hjelme, and H. Korhonen (1993), Earthquake prediction research in the south Iceland seismic zone and the SIL project, *Bull. Seismol. Soc. Am.*, *83*, 696–716.

Stefánsson, R., G. Gudmundsson, and P. Halldórsson (2003), The south Iceland earthquakes 2000—A challenge for earthquake prediction research, *Rep. VI-R03017*, 21 pp., Icelandic Meteorol. Off., Reykjavík.

Sturkell, E., F. Sigmundsson, P. Einarsson, and R. Bilham (1994), Strain accumulation 1986–1992 across the Reykjanes Peninsula plate boundary, Iceland, determined from GPS measurements, *Geophys. Res. Lett.*, *21*, 125–128.

Sturkell, E., F. Sigmundsson, and P. Einarsson (2003), Recent unrest and magma movements at Eyjafjallajäkull and Katla volcanoes, Iceland, *J. Geophys. Res.*, *108*(B8), 2369, doi:10.1029/2001JB000917.

Tryggvason, A., S. T. Rögnvaldsson, and Ó. Flóvenz (2002), Three dimensional imaging of the P- and S-wave velocity structure and earthquake locations beneath southwest Iceland, *Geophys. J. Int.*, *151*, 848–866.

Tse, S. T., and J. R. Rice (1986), Crustal earthquake instability in relation to the depth variation of frictional slip properties, *J. Geophys. Res.*, *91*, 9452–9472.

Vadon, H., and F. Sigmundsson (1997), Crustal deformation from 1992 to 1995 at the Mid-Atlantic Ridge, southwest Iceland, mapped by satellite radar interferometry, *Science*, *275*, 193–197.

Vogfjörd, K. S. (2003), Triggered seismicity in SW Iceland after the June 17, M_w = 6.5 earthquake in the south Iceland seismic zone: The first five mintues, *Geophys. Res. Abstr.*, *5*, Abstract EAE03-A-11251.

Vogfjörd, K. S., H. Geirsson, and E. Sturkell (2004), The August 2003 earthquake swarm near Krisuvik: Fault map from aftershocks and GPS measurements (in Icelandic), paper presented at Spring Meeting 2004, Geosci. Soc. of Iceland, Reykjavik.

Vogfjörd, K. S., S. Hjaltadóttir, and R. Slunga (2005), Volcano-tectonic interaction in the Hengill region, Iceland during 1993–1998, *Geophys. Res. Abstr.*, *7*, Abstract EGU05-J-09947.

Wessel, P., and W. H. F. Smith (1998), New, improved version of generic mapping tools released, *Eos Trans. AGU*, *79*, 47,579.

T. Árnadóttir and E. Sturkell, Nordic Volcanological Center, Institute of Earth Sciences, Askja, Natural Sciences Building, University of Iceland, IS-101 Reykjavík, Iceland. (thora1@hi.is; sturkell@hi.is)

K. L. Feigl, CNRS UMR 5562, 14th Ave Edouard Belin, F-31400 Toulouse, France. (feigl@dtp.obs-mip.fr)

H. Geirsson, Department of Geophysics, Icelandic Meteorological Office, Bústadavegur 9, IS-150 Reykjavík, Iceland. (dori@vedur.is)

W. Jiang, GPS Research Center, Wuhan University 129 Luoyu Road, Wuhan 430079, China. (wpjiang@whu.edu.cn)